

Lamb shift in a light-front Hamiltonian approach

Billy D. Jones and Robert J. Perry

Department of Physics, The Ohio State University, Columbus, Ohio 43210-1106

(Received 9 January 1997)

Light-front Hamiltonian methods are being developed to attack bound-state problems in QCD. In this paper we advance the state of the art for these methods by computing the well-known Lamb shift in hydrogen starting from first principles of QED. There are obvious but significant qualitative differences between QED and QCD. In this paper, we discuss the similarities that may survive in a nonperturbative QCD calculation in the context of a precision nonperturbative QED calculation. Central to the discussion are how a constituent picture arises in a gauge field theory, how bound-state energy scales emerge to guide the renormalization procedure, and how rotational invariance emerges in a light-front calculation. [S0556-2821(97)03012-9]

PACS number(s): 11.10.Ef, 12.20.Ds

I. INTRODUCTION

Why is the calculation of the Lamb shift in hydrogen, which at the level of detail found in this paper was largely completed by Bethe in 1947 [1], of any real interest today? While completing such a calculation using new techniques may be very interesting for formal and academic reasons, our primary motivation is to lay groundwork for precision bound-state calculations in QCD. The Lamb shift provides an excellent pedagogical tool for illustrating light-front Hamiltonian techniques, which are not widely known; but more importantly it presents three of the central dynamical and computational problems that we must face to make these techniques useful for solving QCD: How does a constituent picture emerge in a gauge field theory? How do bound-state energy scales emerge nonperturbatively? How does rotational symmetry emerge in a nonperturbative light-front calculation?

These questions can be answered in detail in QED. The answers clearly change in QCD, and we point out several places where this is clear, but we hope that much of the computational framework successfully employed in QED will survive.

In order to formulate these questions in a more precise fashion, we first outline the general computational strategy we employ. First, we use the renormalization group to produce a regulated effective Hamiltonian H_λ , where λ is a cutoff and renormalization is required to remove cutoff dependence from all physical quantities. At this point we have a regulated Hamiltonian that contains all interactions found in the canonical Hamiltonian, a finite number of new relevant and marginal operators (each of which contains a function of longitudinal momenta because longitudinal locality is not maintained in light-front field theory), and an infinite number of irrelevant operators as would occur in any cutoff theory. This complicated Hamiltonian cannot be directly diagonalized, and since we want to solve bound-state problems we cannot solve it using perturbation theory. The second step is to approximate the full Hamiltonian, using

$$H_\lambda = \mathcal{H}_0 + (H_\lambda - \mathcal{H}_0) \equiv \mathcal{H}_0 + \mathcal{V}, \quad (1)$$

where \mathcal{H}_0 is an approximation that can be solved nonpertur-

batively and \mathcal{V} is treated in bound-state perturbation theory (BSPT). The test of \mathcal{H}_0 is whether BSPT converges or not.

We can now reformulate the questions above. Is there a scale λ at which \mathcal{H}_0 does not require particle emission and absorption? What are the few-body interactions in \mathcal{H}_0 that generate the correct nonperturbative bound-state energy scales? Is there a few-body realization of rotational invariance; and if not, how does rotational symmetry emerge in BSPT? We should emphasize that for our purposes we are primarily interested in answering these questions for low-lying bound states, and refinements may be essential to discuss highly excited states or bound-state scattering.

It is essential that λ , which governs the degree to which states are resolved, be adjusted to obtain a constituent approximation. If λ is kept large with respect to all mass scales in the problem, arbitrarily large numbers of constituents are required in the states because constituent substructure is resolved. A constituent picture can emerge if high-free-energy states couple perturbatively to the low-free-energy states that dominate the low-lying bound-states. In this case the cutoff can be lowered until it approaches the nonperturbative bound-state energy scale and perturbative renormalization may be employed to approximate the effective Hamiltonian. In QED we note that the range into which the cutoff must be lowered is

$$m\alpha^2 \ll \tilde{\lambda} \ll m\alpha, \quad (2)$$

where $\tilde{\lambda} = \lambda - m_p - m_e$ as will be explained later, and m is the reduced mass of hydrogen. If the cutoff is lowered to this range, hydrogen bound-states are well approximated using proton-electron states and including photons and pairs perturbatively.

It is an oversimplification to say the constituent picture emerges because the QED coupling constant is very small. Photons are massless, and regardless of how small α is, one must in principle use a nearly degenerate bound-state perturbation theory that includes extremely low-energy photons nonperturbatively. This is not required in practice, because the Coulomb interaction which sets the important energy scales for the problem produces neutral bound-states from which long wavelength photons effectively decouple. Because of this, even though arbitrarily small energy denomi-

nators are encountered in BSPT due to mixing of electron-proton bound-states and states including extra photons, BSPT can converge because emission and absorption matrix elements vanish sufficiently rapidly.

The well-known answer to the second question above is the two-body Coulomb interaction sets the nonperturbative energy and momentum scales appropriate for QED. We have already used the results of the Bohr scaling analysis that reveals that the bound-state momenta scale as $p \sim m\alpha$ and the energy scales as $E \sim m\alpha^2$. As a result the dominant photon momenta are also of order $m\alpha$, and the corresponding photon energies are of order $m\alpha$. This is what makes it possible to use renormalization to replace photons with effective interactions. The dominant photon energy scale is much greater than the bound-state energy scale, so that λ can be perturbatively lowered into the window in Eq. (2) and photons are not required in the state to leading order. A similar analysis in QCD will reveal qualitatively different results. If a constituent picture emerges, the dominant interaction will be confining and the dominant gluon energy scale will be directly affected by confinement. A confining interaction automatically generates a mass gap for gluon production.

Finally we discuss rotational invariance in a light-front approach. In light-front field theory, boost invariance is kinematic, but rotations about transverse axes involve interactions. Thus rotational invariance is not manifest and all cutoffs violate rotational invariance in light-front field theories. In QED it is easy to see how counterterms in H_λ arise during renormalization that repair this symmetry perturbatively; however, the issue of nonperturbative rotational symmetry is potentially much more complicated. We first discuss leading order BSPT and then turn to higher orders.

To leading order in a constituent picture we require a few-body realization of rotational symmetry. This is simple in nonrelativistic systems, because Galilean rotations and boosts are both kinematic. In QED the constituent momenta in all low-lying bound-states are small, so a nonrelativistic reduction can be used to derive \mathcal{H}_0 . Therefore to leading order in QED we can employ a nonrelativistic realization of rotational invariance. This type of approach can be tried in QCD, but it is not essential that it work because alternative few-body realizations of the full set of Lorentz symmetries exist.

At higher orders in BSPT rotational invariance will not be maintained unless corrections are regrouped. We have computed hyperfine structure and shown that terms from first-order and second-order BSPT are required to obtain angular momentum multiplets [2]. The guiding principle in this and all higher order calculations is to expand not in powers of \mathcal{V} , but in powers of α and $\ln(\alpha)$. \mathcal{H}_0 should provide the leading term in this expansion for BSPT to be well behaved, and subsequent terms should emerge from finite orders of BSPT after appropriate regrouping. Powers of α appear through explicit dependence of interactions on α , and through the dependence of leading order eigenvalues and eigenstates on α introduced by interactions in \mathcal{H}_0 . This second source of dependence can be estimated using the fact that momenta scale as $m\alpha$ in the bound-state wave functions. Of more interest for this paper is the appearance of $\ln(\alpha)$, which is signaled by a divergence in unregulated bound-state

perturbation theory. As has long been appreciated, such logarithms appear when the number of scales contributing to a correction diverges.

The existence of a small parameter simplifies the nonperturbative calculation of bound-state observables considerably, and it has been suggested that a similar expansion be employed to guide light-front QCD calculations even if it requires the introduction of masses that violate rotational invariance away from the critical value of the coupling [3]. We do not detail this proposal, but a thorough understanding of such expansions in QED is almost certainly necessary before one has any hope of using this approach for QCD.

We proceed with a description of our Lamb shift calculation. In hydrogen there is a small amplitude for a bound electron to emit and reabsorb a photon, which leads to a small shift in the binding energy. This is the dominant source of the Lamb shift, and the only part of this shift we compute in this paper. This requires electron self-energy renormalization, but removal of all the bare cutoff $\tilde{\Lambda}$ dependence requires a complete fourth order calculation, which is beyond the scope of this paper. We work with a finite bare cutoff $\tilde{\Lambda} = m\sqrt{2}$, and show that our results are independent of the effective cutoff $\tilde{\lambda}$.

The energy scale for the electron binding energy is $m\alpha^2$, while the scale for photons that couple to the bound states is $m\alpha$. This energy gap makes the theory amenable to the use of effective Hamiltonian techniques. For simplicity, we use a Bloch transformation [4] in this paper to remove the high-energy scale (i.e., $m\alpha$) from the states, and an effective Hamiltonian is derived which acts in the low-energy space alone. This effective Hamiltonian is treated in BSPT, as outlined above. The difference between the $2S_{1/2}$ and the $2P_{1/2}$ energy levels, which are degenerate to lowest order, is calculated.

We divide the calculation into two parts, low- and high-energy intermediate photon contributions. The low-energy photons satisfy $|\mathbf{k}| < \tilde{\lambda}$, while the high-energy intermediate photons satisfy $\tilde{\lambda} < |\mathbf{k}| < m$. $\tilde{\lambda}$ is the effective cutoff for the theory, which is chosen to lie in the range given in Eq. (2). This choice lies between the two dominant energy scales in the problem and allows us to avoid near degeneracy problems. When an actual number is required we use

$$\tilde{\lambda} = \alpha\sqrt{am} \sim 6 \times 10^{-4}m. \quad (3)$$

Note that the spectrum of the exact effective Hamiltonian is independent of $\tilde{\lambda}$, but our approximations introduce $\tilde{\lambda}$ dependence. The range for $\tilde{\lambda}$ is chosen so that the errors appear at a higher order in α than we compute.

One further introductory comment, the high-photon-energy ($\tilde{\lambda} < |\mathbf{k}| < m$) part of the shift is further divided into two regions $\tilde{\lambda} < |\mathbf{k}| < b$ and $b < |\mathbf{k}| < m$, where b is an arbitrary parameter chosen in the range $m\alpha \ll b \ll m$. This simplifies the calculation with appropriate approximations being used in the respective regions. The result must obviously be independent of this arbitrary division point b , and is, unless ‘nonmatching’ approximations are used in the respective regions.

We now outline the paper. In Sec. II we discuss the theoretical framework of this light-front Hamiltonian approach,

and in Sec. III we proceed to discuss the origin of the Coulomb interaction in this framework. Section IV contains the heart of the Lamb shift calculation. In the final section, Sec. V, we summarize and discuss our results.

II. THEORETICAL FRAMEWORK

In this paper, the proton will be treated as a point particle. The Lagrangian for the electron, proton, and photon system is ($e > 0$)

$$\begin{aligned} \mathcal{L} = & -\frac{1}{4} F_{\mu\nu} F^{\mu\nu} + \bar{\psi}_e (i\partial + e\mathbf{A} - m_e) \psi_e \\ & + \bar{\psi}_p (i\partial - e\mathbf{A} - m_p) \psi_p. \end{aligned} \quad (4)$$

The reduced mass of the system is defined in the standard way

$$m = \frac{m_e m_p}{m_e + m_p} = m_e [1 - m_e/m_p + O(1/m_p^2)]. \quad (5)$$

Note that in this paper we take the limit $m_p \rightarrow \infty$ because we are only interested in the dominant part of the Lamb shift. The Lagrangian leads to the following canonical Hamiltonian in the light-cone gauge $A^+ = 0$:

$$H = \int d^2x^\perp dx^- \mathcal{H}, \quad (6)$$

$$\begin{aligned} \mathcal{H} = & \frac{1}{2} (\partial^i A^j)^2 + \xi_e^\dagger (i\sigma^i \partial^i + e\sigma^i A^i - im_e) \\ & \times \frac{1}{i\partial^+} [(i\sigma^i \partial^i + e\sigma^i A^i + im_e) \xi_e] \\ & + \xi_p^\dagger (i\sigma^i \partial^i - e\sigma^i A^i - im_p) \\ & \times \frac{1}{i\partial^+} [(i\sigma^i \partial^i - e\sigma^i A^i + im_p) \xi_p] \\ & - \frac{1}{2} J^+ \frac{1}{(\partial^+)^2} J^+ + J^+ \frac{\partial^i}{\partial^+} A^i. \end{aligned} \quad (7)$$

Note that $i=1,2$ only; $J^+ = 2e(\xi_p^\dagger \xi_p - \xi_e^\dagger \xi_e)$, and σ^i are the standard SU(2) Pauli matrices. The dynamical fields are A^i , ξ_e , and ξ_p , the transverse photon and two-component electron and proton fields, respectively. For the relation between ψ and ξ and a comprehensive summary of our light-front conventions see Appendix A.

The free Hamiltonian is

$$\begin{aligned} h = H|_{(e=0)} = & \int_p \sum_s \left(b_s^\dagger(p) b_s(p) \frac{p^{\perp 2} + m_e^2}{p^+} \right. \\ & \left. + B_s^\dagger(p) B_s(p) \frac{p^{\perp 2} + m_p^2}{p^+} + a_s^\dagger(p) a_s(p) \frac{p^{\perp 2}}{p^+} \right), \end{aligned} \quad (8)$$

plus the antifermions. The notation for our free spectrum is $h|i\rangle = \varepsilon_i|i\rangle$ with $\sum_i |i\rangle\langle i| = 1$, where the sum over i implies a sum over all Fock sectors, momenta, and spin. Next, we

normal order all interactions and neglect zero modes. The canonical interactions from Eq. (7) that we use in this paper are

$$\begin{aligned} v_{1e} = & \int d^2x^\perp dx^- \mathcal{V}_{1e}, \quad v_{1p} = \int d^2x^\perp dx^- \mathcal{V}_{1p}, \\ v_2 = & \int d^2x^\perp dx^- \mathcal{V}_2, \end{aligned} \quad (9)$$

with

$$\begin{aligned} \mathcal{V}_{1e} = & e \xi_e^\dagger \sigma^i A^i \frac{1}{i\partial^+} [(i\sigma^i \partial^i + im_e) \xi_e] \\ & + e \xi_e^\dagger (i\sigma^i \partial^i - im_e) \frac{1}{i\partial^+} [\sigma^i A^i \xi_e] - 2e \xi_e^\dagger \xi_e \frac{\partial^i}{\partial^+} A^i, \end{aligned} \quad (10)$$

$$\begin{aligned} \mathcal{V}_{1p} = & -e \xi_p^\dagger \sigma^i A^i \frac{1}{i\partial^+} [(i\sigma^i \partial^i + im_p) \xi_p] \\ & - e \xi_p^\dagger (i\sigma^i \partial^i - im_p) \frac{1}{i\partial^+} [\sigma^i A^i \xi_p] + 2e \xi_p^\dagger \xi_p \frac{\partial^i}{\partial^+} A^i, \end{aligned} \quad (11)$$

$$\mathcal{V}_2 = -\frac{1}{2} J^+ \frac{1}{(\partial^+)^2} J^+. \quad (12)$$

These are the photon emission and absorption by the electron, photon emission and absorption by the proton, and instantaneous photon interactions, respectively.

Given the canonical Hamiltonian H , we cut off the theory by requiring the free energies of all states to satisfy

$$\varepsilon_i \leq \frac{\mathcal{P}^{\perp 2} + \Lambda^2}{\mathcal{P}^+}, \quad (13)$$

where Λ is the bare cutoff and $\mathcal{P} = (\mathcal{P}^+, \mathcal{P}^\perp)$ is the total momentum of the hydrogen state. Then, with a Bloch transformation we remove the states with free energies satisfying

$$\frac{\mathcal{P}^{\perp 2} + \lambda^2}{\mathcal{P}^+} \leq \varepsilon_i \leq \frac{\mathcal{P}^{\perp 2} + \Lambda^2}{\mathcal{P}^+}, \quad (14)$$

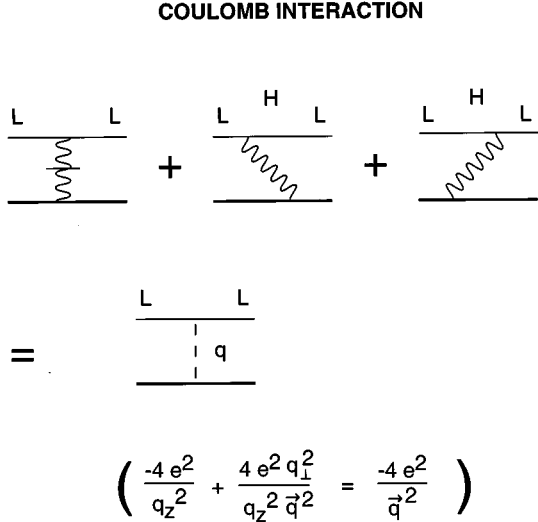
where λ is the effective cutoff. The result is an effective Hamiltonian H_λ acting in the low-energy ($\varepsilon_i \leq \mathcal{P}^{\perp 2}/\mathcal{P}^+ + \lambda^2/\mathcal{P}^+$) space alone. We do not discuss the derivation of H_λ any further, but instead refer the interested reader to Appendix B.

Given H_λ , we then make the following division:

$$H_\lambda = \mathcal{H}_0 + (H_\lambda - \mathcal{H}_0) \equiv \mathcal{H}_0 + \mathcal{V}, \quad (15)$$

where \mathcal{H}_0 is an approximation that can be solved nonperturbatively (for this QED calculation) and \mathcal{V} is treated in BSPT. The test of \mathcal{H}_0 is whether BSPT converges or not and, closely related: is the λ dependence of the spectrum weakened by higher orders of BSPT?

COULOMB INTERACTION



$$\left(\frac{-4e^2}{q_z^2} + \frac{4e^2 q_1^2}{q_z^2 q^2} = \frac{-4e^2}{q^2} \right)$$

FIG. 1. The effective interactions that add to give the Coulomb potential. ‘‘H’’ implies that the photon energy is greater than $\tilde{\lambda}$. ‘‘L’’ implies that the electron kinetic energy is less than $\tilde{\lambda}$. We choose $m\alpha^2 \ll \tilde{\lambda} \ll m\alpha$; these ‘‘H’’ and ‘‘L’’ constraints can thus be removed to leading order.

III. LOWEST ORDER SCHRÖDINGER EQUATION

The primary *assumption* we make in this QED bound-state calculation is that the Coulomb interaction dominates all other physics. In this work we will treat the Coulomb interaction between the electron and proton to all orders in all Fock sectors. After this assumption, the kinematic length scale of our system is fixed,

$$a_0 \sim \frac{1}{p} \sim \frac{1}{m\alpha} \sim \frac{137}{m},$$

which then fixes our dynamical time and length scale,

$$t \sim \frac{1}{p^2/(2m)} \sim \frac{1}{m\alpha^2} \sim \frac{137^2}{m}.$$

As is well known, dynamical changes occur very slowly in this system. Note that in this QED calculation we will treat photons as free since they carry no charge and interact very weakly at low energies. This of course changes drastically for QCD since gluons do carry color charge and interact strongly at low energies. After choosing \mathcal{H}_0 , the α scaling of our BSPT is fixed, and the spectrum is then calculated to some desired order in α and $\ln\alpha$.

In the Coulomb gauge, the Coulomb interaction appears directly in the canonical Hamiltonian, which of course is not true in the light-cone gauge.¹ In the light-cone gauge, the Coulomb interaction arises from a combination of two types of interactions in our effective Hamiltonian, instantaneous photon exchange and the two time orderings of dynamical photon exchange. Graphically this is shown in Fig. 1. These

¹However, a confining potential does appear directly in the canonical Hamiltonian in the light-cone gauge, which is a convenient starting point for QCD [5].

interactions arise from first- and second-order effective interactions, respectively. See Eq. (B10) of Appendix B for the form of the effective Hamiltonian H_λ .

The time-independent Schrödinger equation in light-front coordinates that the sum of the three time-ordered diagrams in Fig. 1 satisfies is²

$$\begin{aligned} & \left(\mathcal{M}_N^2 - \frac{\kappa'^2 + m_e^2}{x'} - \frac{\kappa'^2 + m_p^2}{1-x'} \right) \tilde{\Phi}_N(x' \kappa' s'_e s'_p) \\ & = \sum_{s_e s_p} \int d^2\kappa / (2\pi)^2 \int_0^1 dx / (4\pi) \tilde{V}_c \tilde{\Phi}_N(x \kappa s_e s_p). \end{aligned} \quad (16)$$

\mathcal{M}_N^2 is the mass squared eigenvalue of the state $\tilde{\Phi}_N$, where ‘‘N’’ labels all the quantum numbers of this state. The tildes will be notationally convenient below. We have introduced the following Jacobi variables:

$$p_e = (x\mathcal{P}^+, \kappa + x\mathcal{P}^\perp), \quad (17)$$

$$p'_e = (x'\mathcal{P}^+, \kappa' + x'\mathcal{P}^\perp), \quad (18)$$

where p_e and p'_e are the initial and final electron three-momentum, respectively, and

$$p_e + p_p = p'_e + p'_p = \mathcal{P} = (\mathcal{P}^+, \mathcal{P}^\perp) \quad (19)$$

is the total momentum of the hydrogen state. Note that κ is a two vector. The norm is defined by

$$\begin{aligned} & \sum_{s_e s_p} \int d^2\kappa / (2\pi)^2 \int_0^1 dx / (4\pi) \tilde{\Phi}_N^*(x \kappa s_e s_p) \tilde{\Phi}_N(x \kappa s_e s_p) \\ & = \delta_{NN'}. \end{aligned} \quad (20)$$

\tilde{V}_c is the sum of the interactions given by the three diagrams in Fig. 1, and will not be written in all its gory detail.³ The leading order term of \tilde{V}_c in a nonrelativistic expansion is defined as V_c and is written below.

The nonrelativistic expansion is defined in the following way. A coordinate change which takes the range of longitudinal momentum fraction $x \in [0,1]$ to $\kappa_z \in [-\infty, \infty]$ is defined

$$x = \frac{\kappa_z + \sqrt{\kappa^2 + \kappa_z^2 + m_e^2}}{\sqrt{\kappa^2 + \kappa_z^2 + m_e^2} + \sqrt{\kappa^2 + \kappa_z^2 + m_p^2}}. \quad (21)$$

This step can be taken for relativistic kinematics, but there may be no advantage. Then, the nonrelativistic expansion is an expansion in $|\mathbf{p}|/m$; i.e., we assume

²For a derivation of Eq. (16) from the Schrödinger equation in Fock space see Eqs. (81) to (83) in Sec. III B 1 of Ref. [2].

³The interested reader should consult Eqs. (70) and (71) and the discussion below in Sec. III A 2 of Ref. [2]; these equations are for the equal mass case, but are readily generalized to the unequal mass case. Also note that in this reference we used a similarity transformation instead of a Bloch transformation; the Bloch transformation was chosen for the current paper because of its simplicity.

$$m \gg |\mathbf{p}|, \quad (22)$$

where we have defined a new three vector in terms of our transverse Jacobi variable κ and our new longitudinal momentum variable κ_z which replaces our longitudinal momentum fraction x :

$$\mathbf{p} \equiv (\kappa, \kappa_z). \quad (23)$$

Note that the free mass squared in the Schrödinger equation (16) after this coordinate change, becomes

$$\begin{aligned} \frac{\kappa^2 + m_e^2}{x} + \frac{\kappa^2 + m_p^2}{1-x} &= (\sqrt{m_e^2 + \mathbf{p}^2} + \sqrt{m_p^2 + \mathbf{p}^2})^2 \\ &= (m_e + m_p)^2 + 2(m_e + m_p) \\ &\quad \times \left[\frac{\mathbf{p}^2}{2m} - \frac{\mathbf{p}^4(m_e - m_p)^2}{8mm_e^2m_p^2} + O\left(\frac{|\mathbf{p}|^6}{m^5}\right) \right], \end{aligned} \quad (24)$$

which is invariant under rotations in the space of vectors \mathbf{p} —but not invariant under p_z boosts. Here we begin to see longitudinal boost invariance being replaced by a kinematic rotational invariance in the theory. m is the reduced mass given in Eq. (5).

Now note that the leading order term of \tilde{V}_c in an expansion in $|\mathbf{p}|/m$ is contained in

$$\tilde{V}_c \sim (m_e + m_p)^2 \left(-\frac{4e^2}{q_z^2} + \frac{4e^2 q^{\perp 2}}{q_z^2 \mathbf{q}^2} \theta_H \right) \delta_{s_e s_e'} \delta_{s_p s_p'} \theta_L, \quad (25)$$

where

$$\mathbf{q} = \mathbf{p}' - \mathbf{p}, \quad (26)$$

$$\begin{aligned} \theta_L &= \theta(\lambda^2 - (\sqrt{m_e^2 + \mathbf{p}^2} + \sqrt{m_p^2 + \mathbf{p}^2})^2) \\ &\quad \times \theta(\lambda^2 - (\sqrt{m_e^2 + \mathbf{p}'^2} + \sqrt{m_p^2 + \mathbf{p}'^2})^2), \end{aligned} \quad (27)$$

$$\begin{aligned} \theta_H &= \theta \left[\left((m_e + m_p)^2 + 2(m_e + m_p) \frac{\mathbf{q}^2}{2|q_z|} \right) - \lambda^2 \right] \\ &\quad \times \theta \left[\Lambda^2 - \left((m_e + m_p)^2 + 2(m_e + m_p) \frac{\mathbf{q}^2}{2|q_z|} \right) \right]. \end{aligned} \quad (28)$$

Note that θ_L and θ_H are the constraints that arise from the Bloch transformation.

It is convenient to define new cutoffs which subtract off the total free constituent masses of the state:

$$\tilde{\lambda} \equiv \lambda - (m_e + m_p), \quad (29)$$

$$\tilde{\Lambda} \equiv \Lambda - (m_e + m_p). \quad (30)$$

In the limit $m_p \rightarrow \infty$ we require $\tilde{\lambda}$ and $\tilde{\Lambda}$ to be held fixed. Note that this implies

$$\frac{\lambda^2 - (m_e + m_p)^2}{2(m_e + m_p)} = \tilde{\lambda} + \frac{\tilde{\lambda}^2}{2(m_e + m_p)_{(m_p \rightarrow \infty)}} \sim \tilde{\lambda}, \quad (31)$$

$$\frac{\Lambda^2 - (m_e + m_p)^2}{2(m_e + m_p)} = \tilde{\Lambda} + \frac{\tilde{\Lambda}^2}{2(m_e + m_p)_{(m_p \rightarrow \infty)}} \sim \tilde{\Lambda}. \quad (32)$$

In terms of these new cutoffs, θ_L and θ_H above become

$$\theta_L = \theta \left[\tilde{\lambda} - \frac{\mathbf{p}^2}{2m} + O\left(\frac{|\mathbf{p}|^4}{m^3}\right) \right] \theta \left[\tilde{\lambda} - \frac{\mathbf{p}'^2}{2m} + O\left(\frac{|\mathbf{p}'|^4}{m^3}\right) \right], \quad (33)$$

$$\theta_H = \theta \left(\frac{\mathbf{q}^2}{2|q_z|} - \tilde{\lambda} \right) \theta \left(\tilde{\Lambda} - \frac{\mathbf{q}^2}{2|q_z|} \right). \quad (34)$$

To see the Coulomb interaction arising from the $|ep\rangle$ sector alone, we make the following requirements (which are motivated from the previous two equations):

$$\frac{|\mathbf{p}|^2}{m} \ll \tilde{\lambda} \ll |\mathbf{p}|$$

and

$$\tilde{\Lambda} \gg |\mathbf{p}|, \quad (35)$$

also demanded for $|\mathbf{p}'|$ of course. These constraints will be maintained consistently in this paper. Given these restrictions we have

$$\theta_L \approx 1, \quad (36)$$

$$\theta_H \approx 1. \quad (37)$$

\tilde{V}_c becomes

$$\tilde{V}_c \sim V_c, \quad (38)$$

where

$$\begin{aligned} V_c &\equiv (m_e + m_p)^2 \left(-\frac{4e^2}{q_z^2} + \frac{4e^2 q^{\perp 2}}{q_z^2 \mathbf{q}^2} \right) \delta_{s_e s_e'} \delta_{s_p s_p'} \\ &= -(m_e + m_p)^2 \left(\frac{4e^2}{\mathbf{q}^2} \right) \delta_{s_e s_e'} \delta_{s_p s_p'}. \end{aligned} \quad (39)$$

To finish showing how the Coulomb interaction arises in a light-front Hamiltonian approach, we need to know the Jacobian of the coordinate transformation of Eq. (21):

$$\begin{aligned}
J(p) &= \frac{dx}{d\kappa_z} = \frac{(\kappa_z + \sqrt{\mathbf{p}^2 + m_e^2})(\sqrt{\mathbf{p}^2 + m_p^2} - \kappa_z)}{\sqrt{\mathbf{p}^2 + m_e^2}\sqrt{\mathbf{p}^2 + m_p^2}(\sqrt{\mathbf{p}^2 + m_e^2} + \sqrt{\mathbf{p}^2 + m_p^2})} \\
&= \frac{1}{m_e + m_p} \left[1 + \kappa_z \left(\frac{1}{m_e} - \frac{1}{m_p} \right) - \frac{(\mathbf{p}^2 + 2\kappa_z^2)}{2m_e m_p} + O\left(\frac{|\mathbf{p}|^3}{m^3}\right) \right].
\end{aligned} \tag{40}$$

It is also convenient to redefine the norm:

$$\begin{aligned}
\delta_{NN'} &= \sum_{s_e s_p} \int d^2\kappa / (2\pi)^2 \int_0^1 dx / (4\pi) \tilde{\phi}_{N'}^*(x\kappa s_e s_p) \\
&\quad \times \tilde{\phi}_{N'}(x\kappa s_e s_p) \\
&= \sum_{s_e s_p} \int d^3p J(p) / (16\pi^3) \tilde{\phi}_{N'}^*(\mathbf{p} s_e s_p) \tilde{\phi}_{N'}(\mathbf{p} s_e s_p) \\
&\equiv \sum_{s_e s_p} \int d^3p \phi_N^*(\mathbf{p} s_e s_p) \phi_{N'}(\mathbf{p} s_e s_p).
\end{aligned} \tag{41}$$

In this last line the tildes are removed from the wave functions by defining

$$\phi_N(\mathbf{p} s_e s_p) \equiv \sqrt{\frac{J(p)}{16\pi^3}} \tilde{\phi}_N(\mathbf{p} s_e s_p). \tag{42}$$

Putting it all together, the leading order expression for Eq. (16) in an expansion in $|\mathbf{p}|/m$ given the restrictions of Eq. (35) is

$$\left(-\beta_n + \frac{\mathbf{p}'^2}{2m} \right) \phi_N(\mathbf{p}' s'_e s'_p) = \frac{\alpha}{2\pi^2} \int \frac{d^3p}{(\mathbf{p} - \mathbf{p}')^2} \phi_N(\mathbf{p} s'_e s'_p), \tag{43}$$

which we see is the nonrelativistic Schrödinger equation of hydrogen. m is the reduced mass and $-\beta_n$ is the binding energy defined by

$$\beta_n = \frac{\mathcal{M}_n^2 - (m_e + m_p)^2}{2(m_e + m_p)}. \tag{44}$$

The well-known bound spectrum is

$$\beta_n = -\frac{\text{Ryd}}{n^2}, \tag{45}$$

where $\text{Ryd} = m\alpha^2/2$ of course. Note that Eq. (43) fixes the α scaling of $|\mathbf{p}|$:

$$|\mathbf{p}| \sim m\alpha. \tag{46}$$

Thus we see that the restrictions of Eq. (35) become

$$m\alpha^2 \ll \tilde{\lambda} \ll m\alpha$$

and

$$\tilde{\Lambda} \gg m\alpha, \tag{47}$$

which is consistent with Eq. (2) as advertised earlier.

IV. LAMB SHIFT CALCULATION

Given our lowest order spectrum, we proceed with BSPT. As advertised, this will be divided into *low* and *high* intermediate photon energy calculations. Before proceeding with these respective calculations, we discuss whether Coulomb exchange can be treated perturbatively or nonperturbatively in the respective regions.

For the low-energy intermediate photon, the Coulomb interaction between the intermediate electron and proton must be treated nonperturbatively, whereas this interaction can be treated perturbatively for the high-energy intermediate photon contribution. This is seen by noting that each additional Coulomb exchange contributes a Coulomb matrix element and an energy denominator which is dominated by the larger photon energy scale. Thus each additional Coulomb exchange contributes

$$\frac{\left\langle \frac{\alpha}{|\mathbf{r}|} \right\rangle}{|\mathbf{k}|} \leq \frac{m\alpha^2}{|\mathbf{k}|_{\min}}. \tag{48}$$

For the low-energy photon contribution, in principle $|\mathbf{k}|_{\min}=0$, and each additional Coulomb exchange can contribute order 1, and therefore must be treated nonperturbatively. Of course, when the Coulomb interaction is treated nonperturbatively, low-energy intermediate protons and electrons form bound states from which long-wavelength photons decouple. This nonperturbative effect leads to $|\mathbf{k}|_{\min} \sim 16.64 \text{ Ryd}$; see Eq. (121) below. For the high-energy photon contribution $|\mathbf{k}|_{\min} = \tilde{\lambda}$ and from Eq. (3) each additional Coulomb exchange thus contributes at most

$$\frac{m\alpha^2}{\tilde{\lambda}} = \sqrt{\alpha} \sim 8.5 \times 10^{-2}, \tag{49}$$

and can therefore be treated perturbatively.

A. Low-energy contribution

The low-energy shift arises from two sources which are shown in Fig. 2. The first term comes from the low-energy photon emission part of the effective Hamiltonian $\langle a|v_{1e}|b\rangle$, treated in second-order BSPT. Recall Eqs. (9) and (10) for the form of v_{1e} .⁴ The second term is the result of renormalizing the one loop electron self-energy: a counterterm is added to the second-order self-energy effective interaction in $\langle a|H_\lambda|b\rangle$, which results in a finite (except for in-

⁴Note that the term where the proton emits and subsequently absorbs a photon is down by two powers of the proton mass with respect to the term where the electron emits and absorbs a photon. This result is subtle though, because it is true only after the light-front infrared divergences have canceled between two diagrams analogous to the ones in Fig. 2.

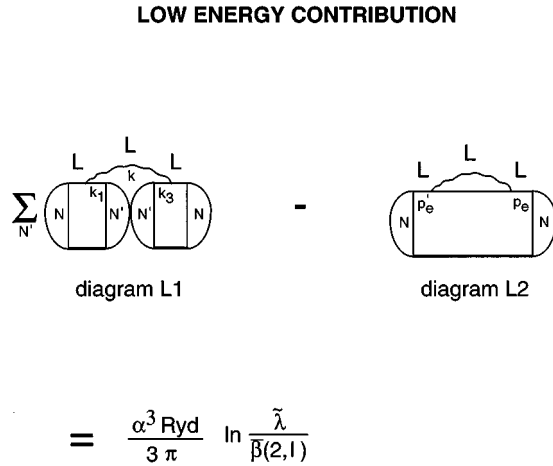


FIG. 2. The low-energy contribution of Sec. IV A. Diagram L1 represents the shift arising from treating photon emission below the cutoff $\tilde{\lambda}$ in second-order BSPT, where the intermediate electron-proton are bound by the Coulomb potential. Diagram L2 is an effective self-energy interaction (plus counterterm), arising from the removal of photon emission above the cutoff $\tilde{\lambda}$, treated in first-order BSPT. $\beta(2,1)$ is the average excitation energy of the $n=2$ state; see Eqs. (115) and (116) and the discussion above them for details.

frared divergences) shift to the electron self-energy. This is shown in Fig. 3. The counterterm is fixed by requiring the electron self-energy to evolve coherently with the cutoff. The details of defining this counterterm, for the equal mass case, can be found in Sec. III A 1 of Ref. [2]. A discussion of the physical ideas behind coupling coherence can be found in Ref. [6], and references therein.

Before proceeding with the calculation, we define the binding energy of hydrogen $-B_N$ in terms of the mass-squared, M_N^2 :

$$M_N^2 = (m_e + m_p + B_N)^2. \quad (50)$$

Assuming B_N is finite as $m_p \rightarrow \infty$ we have

$$\frac{M_N^2 - (m_e + m_p)^2}{2(m_e + m_p)} = B_N + \frac{B_N^2}{2(m_e + m_p)} \sim B_N. \quad (51)$$

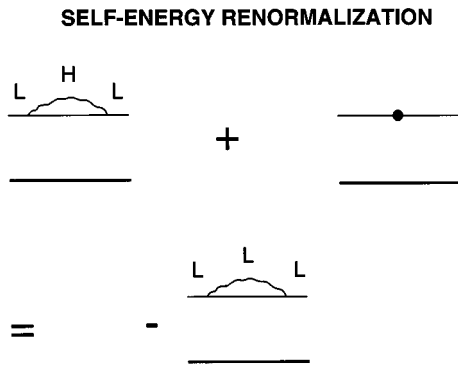


FIG. 3. The sum of an effective self-energy interaction arising from the removal of photon emission above the cutoff $\tilde{\lambda}$ and a counterterm. The counterterm is fixed by coupling coherence. The result is the interaction in diagram L2 of Fig. 2.

Recalling Eq. (44), which is the definition of the zeroth order binding $-\beta_n$ in terms of the zeroth order mass-squared \mathcal{M}_n^2 ; and also defining the mass-squared corrections δM_N^2 by

$$M_N^2 = \mathcal{M}_n^2 + \delta M_N^2, \quad (52)$$

combined with Eq. (51), gives

$$B_N = \beta_n + \frac{\delta M_N^2}{2(m_e + m_p)} \underset{(m_p \rightarrow \infty)}{\sim} \beta_n + \frac{\delta M_N^2}{2m_p}. \quad (53)$$

Defining the binding corrections $-\delta B_N$ by

$$B_N = \beta_n + \delta B_N, \quad (54)$$

combined with Eq. (53), gives

$$\delta B_N = \frac{\delta M_N^2}{2m_p}, \quad (55)$$

a useful formula to be used below. This formula is useful because δM_N^2 is calculated below, but δB_N is the quantity that is measured.

The low-energy calculation proceeds as follows. The first term of Fig. 2 is a second-order BSPT shift which contributes the following to the mass-squared eigenvalue:

$$\delta M_{L1}^2 = \sum_{N'} \int_k \sum_{s_\gamma} \frac{|\langle \psi_N(\mathcal{P}) | v_{1e} a_{s_\gamma}^\dagger(k) | \psi_{N'}(\mathcal{P}-k) \rangle|^2 \theta_{L1}}{\text{DEN}_1(\text{vol})^2}, \quad (56)$$

where k and s_γ are the photon's three-momentum and spin, respectively, $\mathcal{P} = (\mathcal{P}^+, \mathcal{P}^\perp)$ is the total momentum of the hydrogen state ψ_N , and v_{1e} is the photon emission interaction given in Eq. (9). θ_{L1} restricts the energies of the initial, intermediate, and final states to be below the effective cutoff $(\lambda^2 + \mathcal{P}^{\perp 2})/\mathcal{P}^+$. The explicit form of these restrictions is discussed below. Continuing the description of Eq. (56),

$$\int_k = \int \frac{d^2 k^\perp dk^+ \theta(k^+)}{16\pi^3 k^+} = \int \frac{d^3 k}{(2\pi)^3 (2|\mathbf{k}|)}. \quad (57)$$

The last step comes from recalling that for a photon $k^+ = k^0 + k^3 = |\mathbf{k}| + k^3$. The denominator and volume factors are

$$\text{vol} = \int d^2 x^\perp dx^- = 16\pi^3 \delta^3(\mathcal{P} - \mathcal{P}), \quad (58)$$

$$\text{DEN}_1 = \mathcal{P}^+ \left(\frac{\mathcal{P}^{\perp 2} + \mathcal{M}_n^2}{\mathcal{P}^+} - \frac{(\mathcal{P}-k)^{\perp 2} + \mathcal{M}_n^2}{(\mathcal{P}-k)^+} - \frac{k^{\perp 2}}{k^+} \right). \quad (59)$$

The two-body states are

$$|\psi_N(\mathcal{P})\rangle = \int_{p_e p_p} \sqrt{p_e^+ p_p^+} 16\pi^3 \delta^3(\mathcal{P} - p_e - p_p) \times \tilde{\phi}_N(p_e p_p) b_{s_e}^\dagger(p_e) B_{s_p}^\dagger(p_p) |0\rangle, \quad (60)$$

$$|\psi_{N'}(\mathcal{P} - k)\rangle = \int_{k_1 k_2} \sqrt{k_1^+ k_2^+} 16\pi^3 \delta^3(\mathcal{P} - k - k_1 - k_2) \times \tilde{\phi}_{N'}(k_1 k_2) b_{s_e}^\dagger(k_1) B_{s_p}^\dagger(k_2) |0\rangle, \quad (61)$$

where ϕ_N are solutions to Eq. (43), the nonrelativistic Schrödinger equation of hydrogen, and $\tilde{\phi}_N$ is related to ϕ_N by Eq. (42).

Straightforward algebra leads to

$$N_1 = \sum_{s_e' s_\gamma} \frac{\langle 0 | b_{s_e}(p_e') v_{1e} b_{s_e'}^\dagger(k_1) a_{s_\gamma}^\dagger(k) | 0 \rangle \langle 0 | b_{s_e}(k_3) a_{s_\gamma}(k) v_{1e} b_{s_e}^\dagger(p_e) | 0 \rangle}{\sqrt{p_e^+ p_e'^+ k_1^+ k_3^+} (16\pi^3 \delta^3(k + k_3 - p_e)) (16\pi^3 \delta^3(k + k_1 - p_e'))} \quad (63)$$

[for v_{1e} see Eq. (9)], which after some algebra becomes

$$N_1 = (4\pi\alpha) \left[2m_e^2 \left(\frac{1}{p_e^+} - \frac{1}{k_3^+} \right) \left(\frac{1}{p_e'^+} - \frac{1}{k_1^+} \right) + \left(\frac{2k^i}{k^+} - \frac{k_1^i(s_e)}{k_1^+} - \frac{p_e'^i(\bar{s}_e)}{p_e'^+} \right) \times \left(\frac{2k^i}{k^+} - \frac{p_e^i(s_e)}{p_e^+} - \frac{k_3^i(\bar{s}_e)}{k_3^+} \right) \right], \quad (64)$$

where we have defined a new object

$$p^i(s) = p^i + i s \epsilon_{ij} p^j. \quad (65)$$

Notation: $i = 1, 2$ only, $s = \pm 1$ only, $\bar{s} = -s$, $\epsilon_{12} = -\epsilon_{21} = 1$, and $\epsilon_{11} = \epsilon_{22} = 0$.

We now discuss θ_{L1} and then simplify δM_{L1}^2 further. Recall Eqs. (24) and (29). We see that after the coordinate change defined by Eq. (21), in the $m_p \rightarrow \infty$ limit,

$$\theta_{L1} = \theta(\tilde{\lambda} - T_1) \theta\left(\tilde{\lambda} - \frac{\mathbf{p}^2}{2m} + O(\alpha^4)\right) \theta\left(\tilde{\lambda} - \frac{\mathbf{p}'^2}{2m} + O(\alpha^4)\right), \quad (66)$$

$$T_1 = |\mathbf{k}| + \sqrt{(\mathbf{p} - \mathbf{k})^2 + m_e^2} - m_e, \quad (67)$$

where we have used the fact that the wave functions restrict $|\mathbf{p}| \sim m\alpha$. Recall that we are always assuming $m\alpha^2 \ll \tilde{\lambda} \ll m\alpha$. Thus, θ_{L1} can be simplified:

$$\theta_{L1} \approx \theta(\tilde{\lambda} - T_1). \quad (68)$$

$$\delta M_{L1}^2 = \sum_{N'}^c \int_k \int_{p_e} \theta(\mathcal{P}^+ - p_e^+) \int_{p_e'} \theta(\mathcal{P}^+ - p_e'^+) \times \int_{k_1 k_3} (p_e^+ p_e'^+ k_1^+ k_3^+) (16\pi^3 \delta^3(k + k_3 - p_e)) \times (16\pi^3 \delta^3(k + k_1 - p_e')) \tilde{\phi}_N^*(p_e', \mathcal{P} - p_e') \times \tilde{\phi}_{N'}(k_1, \mathcal{P} - k - k_1) \tilde{\phi}_{N'}^*(k_3, \mathcal{P} - k - k_3) \times \tilde{\phi}_N(p_e, \mathcal{P} - p_e) \frac{N_1 \theta_{L1}}{\text{DEN}_1}, \quad (62)$$

where N and N' are shorthands for (n, l, m_l) and (n', l', m_l') , respectively, the usual principal and angular momentum quantum numbers of nonrelativistic hydrogen. The ‘‘c’’ on the sum emphasizes the fact that the continuum states must be included also. See Eq. (59) for DEN_1 . N_1 is given by

From the form of Eq. (67), we see that this constrains the photon momentum to satisfy

$$|\mathbf{k}| \leq \tilde{\lambda}, \quad (69)$$

to leading order in α .

Note that the constraints coming from θ_{L1} , summarized by Eq. (69), require the photon momenta in δM_{L1}^2 of Eq. (62) to satisfy

$$k \ll p_e, p_e'. \quad (70)$$

Thus, Eq. (62) can be simplified further:

$$\delta M_{L1}^2 \approx \sum_{N'}^c \int_k \int_{p_e} \theta(\mathcal{P}^+ - p_e^+) \int_{p_e'} \theta(\mathcal{P}^+ - p_e'^+) \times (p_e^+ p_e'^+) \tilde{\phi}_N^*(p_e', \mathcal{P} - p_e') \times \tilde{\phi}_{N'}(p_e', \mathcal{P} - p_e') \tilde{\phi}_{N'}^*(p_e, \mathcal{P} - p_e) \times \tilde{\phi}_N(p_e, \mathcal{P} - p_e) \frac{N_1}{\text{DEN}_1} \Big|_{(k_3=p_e, k_1=p_e', |\mathbf{k}| \leq \tilde{\lambda})}. \quad (71)$$

In the $m_p \rightarrow \infty$ limit, $\mathcal{P}^+ \rightarrow m_p$, and DEN_1 becomes

$$\text{DEN}_1 = 2m_p (\beta_n - \beta_{n'} - |\mathbf{k}|) [1 + O(1/m_p)], \quad (72)$$

where we have used $k^{\pm 2}/k^+ + k^+ = 2|\mathbf{k}|$, valid for an on-mass-shell photon (all particles in a Hamiltonian approach

are on-mass shell). $-\beta_n$ is the binding energy of nonrelativistic hydrogen defined in Eq. (44), with numerical value Ryd/n^2 for the bound states.

In the region of integration, $|\mathbf{k}| \leq \tilde{\lambda} = m\alpha\sqrt{\alpha} \ll |\mathbf{p}|$, so after the coordinate change of Eq. (21) [recall Eq. (23)] we have

$$\begin{aligned} \frac{N_1}{4\pi\alpha} &= \frac{4k^{\perp 2}}{k^{+2}} + \frac{4k^{\perp 2}}{k^+m} + \frac{4\mathbf{p}^\perp \cdot \mathbf{p}'^\perp}{m^2} \\ &\quad - \frac{4k^\perp}{k^+m} \cdot \left(\mathbf{p}^\perp + \mathbf{p}'^\perp - \frac{\mathbf{p}^\perp p_z}{m} - \frac{\mathbf{p}'^\perp p'_z}{m} \right) + O(\alpha^2\sqrt{\alpha}). \end{aligned} \quad (73)$$

The rest of the integrand is even under $k^\perp \rightarrow -k^\perp$, so these terms in the last line, odd in k^\perp , do not contribute.

Putting it all together, recalling Eq. (55), we have

$$\begin{aligned} \delta B_{L1} &= \frac{\delta M_{L1}^2}{2m_p} \approx \frac{\alpha}{4\pi^2} \sum_{N'}^c \int \frac{d^3k}{|\mathbf{k}|} \theta(\tilde{\lambda} - |\mathbf{k}|) \\ &\quad \times \int d^3p \int d^3p' \phi_N^*(\mathbf{p}') \\ &\quad \times \phi_{N'}(\mathbf{p}') \phi_{N'}^*(\mathbf{p}) \phi_N(\mathbf{p}) \\ &\quad \times \frac{k^{\perp 2}/k^{+2} + k^{\perp 2}/k^+m + (\mathbf{p}^\perp \cdot \mathbf{p}'^\perp)/m^2}{\beta_n - \beta_{n'} - |\mathbf{k}|}, \end{aligned} \quad (74)$$

where we recalled Eq. (42), the relation between ϕ_N and $\tilde{\phi}_N$. This is infrared ($k^+ \rightarrow 0$) divergent, but we must add diagram L2 of Fig. 2 to get the total low-energy shift.

As previously mentioned, Diagram L2 of Fig. 2 arises from the sum of an effective second-order electron self-energy interaction and a counterterm defined such that the electron self-energy runs coherently. The result of this interaction is to add the following to the binding:

$$\begin{aligned} \delta B_{L2} &= \frac{\delta M_{L2}^2}{2m_p} = -\frac{\alpha}{4\pi^2} \sum_{N'}^c \int \frac{d^3k}{|\mathbf{k}|} \theta(\tilde{\lambda} - |\mathbf{k}|) \\ &\quad \times \int d^3p \int d^3p' \phi_N^*(\mathbf{p}') \phi_{N'}(\mathbf{p}') \phi_{N'}^*(\mathbf{p}) \\ &\quad \times \phi_N(\mathbf{p}) \frac{k^{\perp 2}/k^{+2} + k^{\perp 2}/k^+m + (\mathbf{p}^\perp \cdot \mathbf{p}'^\perp)/m^2}{\sqrt{\mathbf{p}^2 + m_e^2} - \sqrt{(\mathbf{p} - \mathbf{k})^2 + m_e^2} - |\mathbf{k}|}. \end{aligned} \quad (75)$$

Given the constraint $|\mathbf{k}| \leq \tilde{\lambda} \ll |\mathbf{p}|$, this becomes

$$\begin{aligned} \delta B_{L2} &\approx \frac{\alpha}{4\pi^2} \sum_{N'}^c \int \frac{d^3k}{|\mathbf{k}|} \theta(\tilde{\lambda} - |\mathbf{k}|) \\ &\quad \times \int d^3p \int d^3p' \phi_N^*(\mathbf{p}') \phi_{N'}(\mathbf{p}') \phi_{N'}^*(\mathbf{p}) \\ &\quad \times \phi_N(\mathbf{p}) \frac{k^{\perp 2}/k^{+2} + k^{\perp 2}/k^+m + (\mathbf{p}^\perp \cdot \mathbf{p}'^\perp)/m^2}{|\mathbf{k}|}. \end{aligned} \quad (76)$$

This is the famous subtraction that Bethe performed in 1947 [1]. In our approach it arose as a consequence of coupling coherence.

δB_{L2} is infrared divergent ($k^+ \rightarrow 0$) as is δB_{L1} . This divergence arises from the first two terms of N_1 (the ones independent of \mathbf{p} and \mathbf{p}'). Noting that

$$|\mathbf{k}| = \frac{1}{2} \left(\frac{k^{\perp 2}}{k^+} + k^+ \right) \underset{(k^+ \rightarrow 0)}{\sim} \frac{k^{\perp 2}}{2k^+},$$

we have

$$\beta_n - \beta_{n'} - |\mathbf{k}| \underset{(k^+ \rightarrow 0)}{\sim} -\frac{k^{\perp 2}}{2k^+},$$

and these infrared divergent contributions from the first two terms of N_1 cancel, leaving an infrared finite shift:

$$\begin{aligned} \delta B_L &= \delta B_{L1} + \delta B_{L2} = \frac{\alpha}{4\pi^2} \sum_{N'}^c \int \frac{d^3k}{|\mathbf{k}|} \theta(\tilde{\lambda} - |\mathbf{k}|) \\ &\quad \times \int d^3p \int d^3p' \phi_N^*(\mathbf{p}') \phi_{N'}(\mathbf{p}') \phi_{N'}^*(\mathbf{p}) \\ &\quad \times \phi_N(\mathbf{p}) \frac{\mathbf{p}^\perp \cdot \mathbf{p}'^\perp}{m^2} \left(\frac{1}{\beta_n - \beta_{n'} - |\mathbf{k}|} + \frac{1}{|\mathbf{k}|} \right) \end{aligned} \quad (77)$$

$$\begin{aligned} &= \left(\frac{2}{3} \right) \frac{\alpha}{4\pi^2} \sum_{N'}^c \int \frac{d^3k}{|\mathbf{k}|} \theta(\tilde{\lambda} - |\mathbf{k}|) \int d^3p \\ &\quad \times \int d^3p' \phi_N^*(\mathbf{p}') \phi_{N'}(\mathbf{p}') \phi_{N'}^*(\mathbf{p}) \\ &\quad \times \phi_N(\mathbf{p}) \frac{\mathbf{p} \cdot \mathbf{p}'}{m^2} \left(\frac{1}{\beta_n - \beta_{n'} - |\mathbf{k}|} + \frac{1}{|\mathbf{k}|} \right). \end{aligned} \quad (78)$$

This last step followed after averaging over directions as dictated by rotational invariance.

Equation (78) is easy to integrate, and our final result for the low-energy photon contribution is

$$\begin{aligned} \delta B_L &= \frac{2\alpha}{3\pi m^2} \sum_{N'}^c (\beta_{n'} - \beta_n) \ln \left| \frac{\tilde{\lambda} + \beta_{n'} - \beta_n}{\beta_{n'} - \beta_n} \right| |\langle \phi_N | \hat{\mathbf{p}} | \phi_{N'} \rangle|^2 \\ &= \frac{2\alpha}{3\pi m^2} \sum_{N'}^c (\beta_{n'} - \beta_n) \ln \left| \frac{\tilde{\lambda}}{\beta_{n'} - \beta_n} \right| |\langle \phi_N | \hat{\mathbf{p}} | \phi_{N'} \rangle|^2, \end{aligned} \quad (79)$$

(80)

where in this last step we recalled $\tilde{\lambda} \gg m\alpha^2$. Note the $\tilde{\lambda}$ dependence in the result. This will cancel after we correctly add the contributions coming from high energy intermediate photons, which now follows.

B. High-energy contribution

The high-energy shift arises from three sources which are shown in Fig. 4. These are first-order BSPT shifts due to third and fourth order effective interactions (see Appendix B). The net result of these three diagrams is

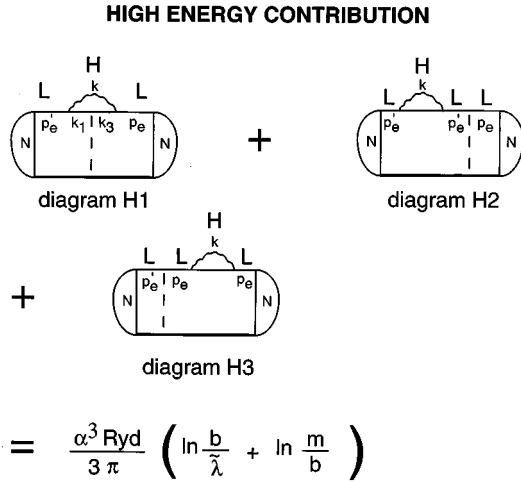


FIG. 4. The high-energy contribution of Sec. IV B. These are third- and fourth-order effective interactions treated in first-order BSPT. These effective interactions arise from the removal of photon emission above the cutoff $\tilde{\lambda}$. ‘‘ b ’’ is an arbitrary scale, required to satisfy $m\alpha \ll b \ll m$, that was introduced to simplify the calculation. Note the b independence of the result. The total contribution is a sum of Fig. 2 and Fig. 4. Note the $\tilde{\lambda}$ independence of the combined result.

$$-\frac{\alpha}{2\pi^2 \mathbf{q}^2} \rightarrow -\frac{\alpha}{2\pi^2 \mathbf{q}^2} (1 + \delta V_H), \quad (81)$$

where \mathbf{q} is the exchanged momentum of the electron, and

$$\delta V_H = \delta V_{H1} + \delta V_{H2} + \delta V_{H3}, \quad (82)$$

with

$$\begin{aligned} \delta V_{H1} = & \frac{1}{2} \int_k \theta(p_e'^+ - k^+) \theta(p_e^+ - k^+) N_{H1} \theta_{H1} \\ & \times \left(\frac{(\mathcal{P}^+)^2}{(M_0^2 - M^2)(M_0^2 - M'^2)} \right. \\ & \left. + \frac{(\mathcal{P}^+)^2}{(M_0'^2 - M^2)(M_0'^2 - M'^2)} \right), \quad (83) \end{aligned}$$

$$\begin{aligned} \delta V_{H2} = & -\frac{1}{2} \int_k \theta(p_e'^+ - k^+) \theta(p_e^+ - k^+) N_{H2} \theta_{H2} \\ & \times \frac{(\mathcal{P}^+)^2}{(M_0^2 - M'^2)(M_0'^2 - M'^2)}, \quad (84) \end{aligned}$$

$$\begin{aligned} \delta V_{H3} = & -\frac{1}{2} \int_k \theta(p_e'^+ - k^+) \theta(p_e^+ - k^+) N_{H3} \theta_{H3} \\ & \times \frac{(\mathcal{P}^+)^2}{(M_0^2 - M^2)(M_0'^2 - M^2)}. \quad (85) \end{aligned}$$

The factors $\pm \frac{1}{2}$ in front arise from the form of the Bloch transformation [see Eq. (B10) of Appendix B]. The vertex factors are given by

$$N_{H1} = (N_1)_{(k_1 \rightarrow p_e' - k, k_3 \rightarrow p_e - k)}, \quad (86)$$

$$N_{H2} = (N_1)_{(k_1 \rightarrow p_e' - k, k_3 \rightarrow p_e' - k, p_e \rightarrow p_e')}, \quad (87)$$

$$N_{H3} = (N_1)_{(k_1 \rightarrow p_e - k, k_3 \rightarrow p_e - k, p_e' \rightarrow p_e)}, \quad (88)$$

where N_1 was defined in Eq. (64). The free state masses are given by

$$M_0 = \sqrt{\mathbf{p}^2 + m_e^2} + \sqrt{\mathbf{p}^2 + m_p^2}, \quad (89)$$

$$M'_0 = \sqrt{\mathbf{p}'^2 + m_e^2} + \sqrt{\mathbf{p}'^2 + m_p^2}, \quad (90)$$

$$M = |\mathbf{k}| + \sqrt{(\mathbf{p} - \mathbf{k})^2 + m_e^2} + \sqrt{\mathbf{p}^2 + m_p^2}, \quad (91)$$

$$M' = |\mathbf{k}| + \sqrt{(\mathbf{p}' - \mathbf{k})^2 + m_e^2} + \sqrt{\mathbf{p}'^2 + m_p^2}. \quad (92)$$

The Bloch transformation constrains the free masses of the states. As discussed before, the ‘‘L’’ restrictions in Fig. 4 can be removed given $\tilde{\lambda} \gg m\alpha^2$. However, the ‘‘H’’ restrictions lead to important constraints given by the θ_H factors above, which we now discuss. They constrain the free masses to satisfy [recall Eqs. (29)–(32)]

$$\tilde{\lambda} \leq M - m_e - m_p \leq \tilde{\Lambda}, \quad (93)$$

$$\tilde{\lambda} \leq M' - m_e - m_p \leq \tilde{\Lambda}, \quad (94)$$

where M and M' are defined in Eqs. (91) and (92), respectively.

As already mentioned, for convenience of calculation, we will divide this high-energy contribution into two regions, $\tilde{\lambda} \leq |\mathbf{k}| \leq b$ and $b \leq |\mathbf{k}| \leq m$ (*region one* and *region two*, respectively), with $m\alpha \ll b \sim m\sqrt{\alpha} \ll m$. Recall, $m\alpha^2 \ll \tilde{\lambda} \sim m\alpha\sqrt{\alpha} \ll m\alpha$. We now show how this division into these two regions arises as a result of the constraints of Eqs. (93) and (94).

In this first region $|\mathbf{k}| \ll m$, and Eqs. (93) and (94) become

$$\tilde{\lambda} \leq |\mathbf{k}| + \frac{(\mathbf{p} - \mathbf{k})^2}{2m} \sim |\mathbf{k}| \leq b, \quad (95)$$

$$\tilde{\lambda} \leq |\mathbf{k}| + \frac{(\mathbf{p}' - \mathbf{k})^2}{2m} \sim |\mathbf{k}| \leq b, \quad (96)$$

which is as we have already stated (recall that we always assume $m_p \rightarrow \infty$ and drop the $1/m_p$ corrections since we are just after the dominant shift).

The analysis of the second region is slightly more complicated because $|\mathbf{k}| \gg m\alpha$, and near the upper limit $|\mathbf{k}| \sim m$. Since $|\mathbf{k}| \gg m\alpha$ in this region, Eqs. (93) and (94) both become

$$b \leq |\mathbf{k}| + \sqrt{\mathbf{k}^2 + m^2} - m \leq \tilde{\Lambda}. \quad (97)$$

This is just a linear constraint,

$$b \left(\frac{2m + b}{2m + 2b} \right) \leq |\mathbf{k}| \leq \frac{\tilde{\Lambda}}{2} \left(\frac{\tilde{\Lambda} + 2m}{\tilde{\Lambda} + m} \right), \quad (98)$$

which, since we choose $b \ll m$, becomes

$$b \ll |\mathbf{k}| \leq \frac{\tilde{\Lambda}}{2} \left(\frac{\tilde{\Lambda} + 2m}{\tilde{\Lambda} + m} \right). \quad (99)$$

The electron self-energy renormalization is performed in this paper, but we do not deal with removing the full $\tilde{\Lambda}$ dependence. A full analysis of this dependence requires a complete fourth order calculation, which is beyond the scope of this paper. We cut off the photon momentum at the electron mass, and proceed. Note that from Eq. (99), this choice corresponds to $\tilde{\Lambda}^2 = 2m^2$. The point of calculating these high-photon-energy contributions is to show that our results are independent of the effective cutoff $\tilde{\lambda}$.

Taking a sample denominator we have

$$\begin{aligned} (M_0^2 - M^2) &= (M_0 + M)(M_0 - M) \\ &\approx 2m_p \left(\frac{\mathbf{p}^2}{2m} - |\mathbf{k}| - \frac{(\mathbf{p} - \mathbf{k})^2}{2m} \right) \\ &\approx -2m_p |\mathbf{k}|, \end{aligned} \quad (100)$$

in the *first* region and

$$\begin{aligned} (M_0^2 - M^2) &= (M_0 + M)(M_0 - M) \\ &\approx 2m_p (m - |\mathbf{k}| - \sqrt{\mathbf{k}^2 + m^2}) \\ &\approx -2m_p \left(|\mathbf{k}| + \frac{|\mathbf{k}|^2}{2m} \right), \end{aligned} \quad (101)$$

in the *second* region.

Using these previous formulas, including $\mathcal{P}^+ \rightarrow m_p$ as $m_p \rightarrow \infty$, Eqs. (83)–(85), after summing, become

$$\delta V_H' = -\frac{\alpha}{4\pi} \frac{q^{\perp 2}}{m^2} \int_{-1}^1 d\cos\theta \int_{\tilde{\lambda}}^{bd|\mathbf{k}|} \frac{d|\mathbf{k}|}{|\mathbf{k}|} \left[1 + O\left(\frac{|\mathbf{k}|}{m}\right) \right], \quad (102)$$

in the first region (the ‘‘prime’’ on δV_H signifies the *first* region) and

$$\begin{aligned} \delta V_H'' &= -\frac{\alpha}{4\pi} \frac{q^{\perp 2}}{m^2} \int_{-1}^1 d\cos\theta \int_b^{md|\mathbf{k}|} \frac{d|\mathbf{k}|}{|\mathbf{k}|} \left[1 + c_n \frac{|\mathbf{k}|}{m} (1 + \cos\theta) \right. \\ &\quad \left. - c_d \frac{|\mathbf{k}|}{m} + O\left(\frac{|\mathbf{k}|^2}{m^2}\right) \right], \end{aligned} \quad (103)$$

in the second region (the ‘‘double prime’’ on δV_H signifies the *second* region). In the second region since the photon momentum is not necessarily smaller than the electron mass, we have kept two terms in the $|\mathbf{k}|/m$ expansion of the integrand. In the $O(|\mathbf{k}|/m)$ term we have introduced two constants c_n and c_d , which denote *numerator* and *energy denominator* corrections, respectively. Hereafter we set $c_n = 1$ and $c_d = 1$, as given by the theory. Note that in combining δV_{H1} , δV_{H2} , and δV_{H3} , many cancellations occur; most noteworthy, each contribution is individually infrared divergent ($k^+ \rightarrow 0$), but in the sum the divergences cancel. These final equations are easily integrated, and we have

$$\delta V_H' = -\frac{\alpha}{2\pi} \frac{q^{\perp 2}}{m^2} \ln\left(\frac{b}{\tilde{\lambda}}\right), \quad (104)$$

$$\delta V_H'' = -\frac{\alpha}{2\pi} \frac{q^{\perp 2}}{m^2} \ln\left(\frac{m}{b}\right). \quad (105)$$

In the second region note that the $O(|\mathbf{k}|/m)$ terms coming from numerator and energy denominator corrections cancel, leaving the order 1 piece alone. The combined high-energy contribution is

$$\delta V_H = \delta V_H' + \delta V_H'' = -\frac{\alpha}{2\pi} \frac{q^{\perp 2}}{m^2} \ln\left(\frac{m}{\tilde{\lambda}}\right), \quad (106)$$

which is independent of b , as required for consistency. Recall that $\mathbf{q} = \mathbf{p}' - \mathbf{p}$: the difference between the final and initial electron momenta.

From the definition of δV_H [see Eq. (81)], we see that this correction shifts the energy levels an amount

$$\delta B_H = -\frac{\alpha}{2\pi^2} \int d^3p d^3p' \phi_N^*(\mathbf{p}') \left(\frac{\delta V_H}{(\mathbf{p} - \mathbf{p}')^2} \right) \phi_N(\mathbf{p}). \quad (107)$$

Combining this with Eq. (106) gives

$$\begin{aligned} \delta B_H &= \frac{\alpha^2}{4\pi^3 m^2} \ln\left(\frac{m}{\tilde{\lambda}}\right) \int d^3p d^3p' \phi_N^*(\mathbf{p}') \\ &\quad \times \left(\frac{(\mathbf{p}^\perp - \mathbf{p}'^\perp)^2}{(\mathbf{p} - \mathbf{p}')^2} \right) \phi_N(\mathbf{p}) \end{aligned} \quad (108)$$

$$= \frac{\alpha^2}{6\pi^3 m^2} \ln\left(\frac{m}{\tilde{\lambda}}\right) \left(\int d^3p \phi_N(\mathbf{p}) \right)^2, \quad (109)$$

where in this last step we averaged over directions and noted that the wave function at the origin is real. For more details on this averaging over directions see Appendix C.

C. Total contribution

In this section we combine the results of the last two sections for the low- and high-photon energy contributions, and perform the required sums and integrations to calculate the total shift between the $2S_{1/2}$ and $2P_{1/2}$ energy levels of hydrogen.

Adding Eqs. (80) and (109) gives for the total shift

$$\begin{aligned} \delta B &= \delta B_L + \delta B_H \\ &= \frac{2\alpha}{3\pi m^2} \sum_{N'}^c (\beta_{n'} - \beta_n) \ln \left| \frac{\tilde{\lambda}}{\beta_{n'} - \beta_n} \right| |\langle \phi_N | \hat{\mathbf{p}} | \phi_{N'} \rangle|^2 \\ &\quad + \frac{\alpha^2}{6\pi^3 m^2} \ln\left(\frac{m}{\tilde{\lambda}}\right) \left(\int d^3p \phi_N(\mathbf{p}) \right)^2. \end{aligned} \quad (110)$$

For the second term we have

$$\begin{aligned} \left(\int d^3p \phi_N(\mathbf{p}) \right)^2 &= ((2\pi)^{3/2} \phi_N(\mathbf{x}=0))^2 \\ &= \frac{(2\pi)^3}{\pi} \left(\frac{m\alpha}{n} \right)^3 \delta_{l,0}. \end{aligned} \quad (111)$$

The $(2\pi)^3$ factor arose because of our normalization choice [see Eq. (41)].

The first term of Eq. (110) is the famous Bethe log and must be calculated numerically, summing over all bound and continuum states. Following standard convention we define an average excitation energy $\bar{\beta}(n,l)$:

$$\begin{aligned} \ln \left(\frac{\bar{\beta}(n,l)}{\text{Ryd}} \right) \sum_{N'}^c (\beta_{n'} - \beta_n) |\langle \phi_N | \hat{\mathbf{p}} | \phi_{N'} \rangle|^2 \\ = \sum_{N'}^c (\beta_{n'} - \beta_n) \ln \left| \frac{\beta_{n'} - \beta_n}{\text{Ryd}} \right| |\langle \phi_N | \hat{\mathbf{p}} | \phi_{N'} \rangle|^2. \end{aligned} \quad (112)$$

The sum on the left is evaluated by standard techniques [$H_c = p^2/(2m) - \alpha/r$]:

$$\begin{aligned} \sum_{N'}^c (\beta_{n'} - \beta_n) |\langle \phi_N | \hat{\mathbf{p}} | \phi_{N'} \rangle|^2 \\ = \frac{1}{2} \langle \phi_N | [\hat{\mathbf{p}}, H_c] \cdot \hat{\mathbf{p}} + \hat{\mathbf{p}} \cdot [H_c, \hat{\mathbf{p}}] | \phi_N \rangle \\ = -\frac{1}{2} \langle \phi_N | [\hat{\mathbf{p}} \cdot, [\hat{\mathbf{p}}, H_c]] | \phi_N \rangle \\ = -\frac{1}{2} \langle \phi_N | [\hat{\mathbf{p}} \cdot, -i\vec{\nabla}(-\alpha/r)] | \phi_N \rangle \\ = -\frac{1}{2} \langle \phi_N | (-i)^2 \vec{\nabla}^2(-\alpha/r) | \phi_N \rangle \\ = -\frac{1}{2} (-i)^2 (-\alpha) (-4\pi) \langle \phi_N | \delta^3(r) | \phi_N \rangle \\ = 2\alpha \left(\frac{m\alpha}{n} \right)^3 \delta_{l,0}. \end{aligned} \quad (113)$$

This vanishes for $l \neq 0$, but the average excitation energy $\bar{\beta}(n,l)$ is defined [it is just a way to catalogue the numerical sum on the right of Eq. (112), the quantity we need to know] with the sum on the left-hand side set to its value for $l=0$. In summary, $\bar{\beta}(n,l)$ for all states is defined by

$$\begin{aligned} \ln \left(\frac{\bar{\beta}(n,l)}{\text{Ryd}} \right) 2\alpha \left(\frac{m\alpha}{n} \right)^3 \\ = \sum_{N'}^c (\beta_{n'} - \beta_n) \ln \left| \frac{\beta_{n'} - \beta_n}{\text{Ryd}} \right| |\langle \phi_N | \hat{\mathbf{p}} | \phi_{N'} \rangle|^2. \end{aligned} \quad (114)$$

Without further ado, this sum has been evaluated by Huff [8]. His results for the $n=2$ levels are

$$\bar{\beta}(2,0) = 16.639\,342\,03(1) \text{ Ryd}, \quad (115)$$

$$\bar{\beta}(2,1) = 0.970\,429\,318\,6(3) \text{ Ryd}, \quad (116)$$

where the figures in parentheses give the number of units of estimated error in the last decimal place (Huff's estimates). Combining the results,

$$\begin{aligned} \delta B_{2S_{1/2}} &= \frac{2\alpha}{3\pi m^2} \ln \left(\frac{\tilde{\lambda}}{\bar{\beta}(2,0)} \right) 2\alpha \left(\frac{m\alpha}{n} \right)^3 \\ &\quad + \frac{\alpha^2}{6\pi^3 m^2} \ln \left(\frac{m}{\tilde{\lambda}} \right) \frac{(2\pi)^3}{\pi} \left(\frac{m\alpha}{n} \right)^3 \\ &= \frac{\alpha^3 \text{Ryd}}{3\pi} \ln \left(\frac{m}{\bar{\beta}(2,0)} \right), \end{aligned} \quad (117)$$

$$\begin{aligned} \delta B_{2P_{1/2}} &= \frac{2\alpha}{3\pi m^2} \ln \left(\frac{\text{Ryd}}{\bar{\beta}(2,1)} \right) 2\alpha \left(\frac{m\alpha}{n} \right)^3 \\ &= \frac{\alpha^3 \text{Ryd}}{3\pi} \ln \left(\frac{\text{Ryd}}{\bar{\beta}(2,1)} \right). \end{aligned} \quad (118)$$

Note the cancellation of the $\tilde{\lambda}$ dependence. Thus, the Lamb shift is

$$\begin{aligned} \delta B_{\text{Lamb}} &= \delta B_{2S_{1/2}} - \delta B_{2P_{1/2}} = \frac{\alpha^3 \text{Ryd}}{3\pi} \ln \left(\frac{m\bar{\beta}(2,1)}{\text{Ryd}\bar{\beta}(2,0)} \right) \\ &= (1047 - 4) \text{ MHz } (2\pi\hbar) = 1043 \text{ MHz } (2\pi\hbar), \end{aligned} \quad (119)$$

$$(120)$$

where we use Ref. [9] and the average excitation energies of Eqs. (115) and (116). Note that the $2P_{1/2}$ shift is only about one half of a percent of the $2S_{1/2}$ shift.

V. SUMMARY AND DISCUSSION

In a light-front Hamiltonian approach, we have shown how to do a consistent Lamb shift calculation for the $n=2$, $j=1/2$ levels of hydrogen over the photon energy scales

$$0 \leftrightarrow m\alpha^2 \leftrightarrow \tilde{\lambda} \leftrightarrow m\alpha \leftrightarrow b \leftrightarrow m,$$

with the choices $m\alpha^2 \ll \tilde{\lambda} \ll m\alpha$ and $m\alpha \ll b \ll m$. In a consistent set of diagrams we showed how $\tilde{\lambda}$ and b dependence cancel leaving the dominant part of the Lamb shift, 1043 MHz. For completeness, the $n=2$ spectrum of hydrogen is shown in Fig. 5.

If we compare the three regions we see the following results (we only compare for the $2S_{1/2}$ shift since the $2P_{1/2}$ shift is negligible within our errors):

$$\begin{aligned} (0 \leq |\mathbf{k}| \leq \tilde{\lambda}) \delta B_{\text{Lamb}} &\sim \frac{\alpha^3 \text{Ryd}}{3\pi} \ln \left(\frac{\tilde{\lambda}}{16.64 \text{ Ryd}} \right) \\ &\sim 46 \text{ MHz } (2\pi\hbar) \sim 4\%, \end{aligned} \quad (121)$$

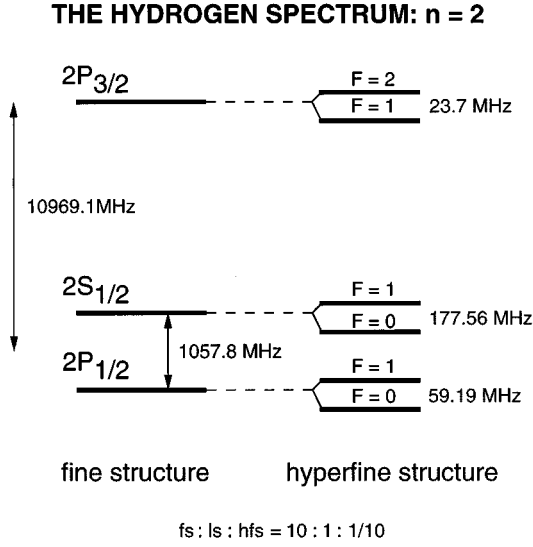


FIG. 5. The $n=2$ hydrogen spectrum: fine structure, Lamb shift, and hyperfine structure. $\mathbf{F}=\mathbf{L}+\mathbf{S}_e+\mathbf{S}_p$.

$$\begin{aligned} (\tilde{\lambda} \leq |\mathbf{k}| \leq b) \delta B_{\text{Lamb}} &\sim \frac{\alpha^3 \text{Ryd}}{3\pi} \ln\left(\frac{b}{\tilde{\lambda}}\right) \sim 667 \text{ MHz} \quad (2\pi\hbar) \\ &\sim 64\%, \end{aligned} \quad (122)$$

$$\begin{aligned} (b \leq |\mathbf{k}| \leq m) \delta B_{\text{Lamb}} &\sim \frac{\alpha^3 \text{Ryd}}{3\pi} \ln\left(\frac{m}{b}\right) \sim 334 \text{ MHz} \quad (2\pi\hbar) \\ &\sim 32\%, \end{aligned} \quad (123)$$

where we used $\tilde{\lambda} = m\alpha\sqrt{\alpha}$ and $b = m\sqrt{\alpha}$, consistent choices used throughout this paper. As expected on physical grounds (see the Introduction), photons with momentum

$$|\mathbf{k}| \sim 1/a_0 \sim m\alpha, \quad (124)$$

couple the strongest to the hydrogen system. As seen above, the effects of photons of this momentum amounted to about 2/3 of the Lamb shift, the dominant part of this experimentally observed shift.

In this paper, the one loop electron self-energy renormalization was performed. The complete one loop renormalization was not needed to obtain the dominant part of the Lamb shift. Our answer, 1043 MHz, turned out to be accurate. However, to obtain more precision, the full one loop renormalization must be performed of course. Also, each of our five diagrams (of Figs. 2 and 4) were infrared ($k_{\text{photon}}^+ \rightarrow 0$) divergent. However, both the sum of the two low-photon-energy diagrams and the sum of the three high-photon-energy diagrams were infrared finite.

The state of the art for the bound-state problem in a light-front Hamiltonian gauge theory in four dimensions has been advanced in this paper. In applying these methods to QCD, the general computational strategy described in the Introduction does not change. However, gluons carry color charge and interact strongly at low energies, thus the answers to the three questions posed in the initial paragraph of the Introduction change drastically. For a constituent picture to emerge the massless gluons must be confined, so that it costs energy

to add a low-momentum gluon to the system.⁵ It has been shown that the second order effective interactions (including the very important first order instantaneous-gluon potential) are confining [5], which is promising. Given confinement, we can lower the effective cutoff below the gluon production threshold perturbatively and obtain a constituent approximation. As in QED, we cannot lower the effective cutoff below the nonperturbative bound-state energy scale. Thus Eq. (2) of hydrogen in QCD becomes

$$\Lambda_{\text{QCD}} \ll \tilde{\lambda} \ll E_{\text{gluon}} \sim M_{\text{glueball}}/2. \quad (125)$$

Since Λ_{QCD} ranges from 200–400 MeV (depending on the renormalization scheme that is chosen) and M_{glueball} ranges from 1500–1700 MeV, this constraint can be satisfied and it becomes plausible to attack QCD by the same computational strategy that was outlined and carried out for the Lamb shift in QED in this paper.

ACKNOWLEDGMENTS

The authors wish to acknowledge useful discussions with Brent H. Allen, Martina M. Brisudová, Stanisław D. Głazek, Koji Harada, and Kenneth G. Wilson. The research reported in this paper has been supported by the National Science Foundation under Grant No. PHY-9409042.

APPENDIX A: LIGHT-FRONT CONVENTIONS

In this appendix we write our light-front conventions for the electron, proton, and photon system:

$$V^\pm = V^0 \pm V^3, \quad \text{where } V^\mu \text{ is any four vector.}$$

$$\gamma^+ = \begin{bmatrix} 0 & 0 \\ 2i & 0 \end{bmatrix}; \quad \gamma^- = \begin{bmatrix} 0 & -2i \\ 0 & 0 \end{bmatrix}.$$

$$\alpha^i = \gamma^0 \gamma^i = \begin{bmatrix} 0 & \sigma^i \\ \sigma^i & 0 \end{bmatrix};$$

$i=1,2$; σ^i are SU(2) Pauli matrices.

$$\Lambda_+ = \frac{1}{2} \gamma^0 \gamma^+ = \begin{bmatrix} 1 & 0 \\ 0 & 0 \end{bmatrix}; \quad \Lambda_- = \frac{1}{2} \gamma^0 \gamma^- = \begin{bmatrix} 0 & 0 \\ 0 & 1 \end{bmatrix}.$$

$$\psi_\pm = \Lambda_\pm \psi; \quad \psi = \psi_+ + \psi_-.$$

$$\psi_{e+} = \begin{bmatrix} \xi_e \\ 0 \end{bmatrix}; \quad \psi_{p+} = \begin{bmatrix} \xi_p \\ 0 \end{bmatrix}; \quad e \text{ for electron, } p \text{ for proton.}$$

$$\psi_{e-} = \begin{bmatrix} 0 \\ \frac{1}{i\partial^+} [(\sigma^i (i\partial^i + eA^i) + im_e)\xi_e] \end{bmatrix}.$$

⁵The energy of this confined low momentum gluon can be interpreted as an effective gluon mass if it is convenient.

$$\psi_{p^-} = \begin{bmatrix} 0 \\ \frac{1}{i\partial^+} [(\sigma^i(i\partial^i - eA^i) + im_p)\xi_p] \end{bmatrix}.$$

$$A^- = \frac{-2}{(\partial^+)^2} J^+ + 2\frac{\partial^i}{\partial^+} A^i.$$

$$J^+ = 2e(\xi_p^\dagger \xi_p - \xi_e^\dagger \xi_e); \quad e > 0.$$

$$A^+ = 0.$$

In momentum space the field operators are expanded as (at $x^+ = 0$):

$$A^i(x) = \sum_{s=\pm 1} \int_q (\epsilon_s^i a_s(q) e^{-iq \cdot x} + \text{H.c.}),$$

$$\xi_e(x) = \sum_{s=\pm 1} \chi_s \int_p \sqrt{p^+} (b_s(p) e^{-ip \cdot x} + d_s^\dagger(p) e^{+ip \cdot x}),$$

$$\xi_p(x) = \sum_{s=\pm 1} \chi_s \int_p \sqrt{p^+} (B_s(p) e^{-ip \cdot x} + D_s^\dagger(p) e^{+ip \cdot x}),$$

with

$$\epsilon_1^i = \frac{-1}{\sqrt{2}} (\delta_{i,1} + i\delta_{i,2}), \quad \epsilon_{-1}^i = \frac{1}{\sqrt{2}} (\delta_{i,1} - i\delta_{i,2}),$$

$$\chi_1 = \begin{pmatrix} 1 \\ 0 \end{pmatrix}, \quad \chi_{-1} = \begin{pmatrix} 0 \\ 1 \end{pmatrix}.$$

Note that $\bar{s} \equiv -s$. Also, we are using the shorthand

$$\int_p f(p) = \int \frac{d^4 p}{(2\pi)^4} 2\pi \delta(p^2 - m^2) \theta(p^0) f(p)$$

$$= \int \frac{d^2 p^\perp dp^+ \theta(p^+)}{16\pi^3 p^+} f(p)|_{p^- = (p^\perp{}^2 + m^2)/p^+}.$$

The fermion helicity can only take on the values $\pm 1/2$, however, we define $h_3 = s/2$; therefore, “ s ” can only take on the values ± 1 . The commutation (anticommutation) relations and free Fock states are given by

$$[a_\lambda(q), a_\lambda^\dagger(q')] = 16\pi^3 q^+ \delta^3(q - q') \delta_{\lambda\lambda'}$$

$$(\delta^3(p) = \delta^2(p^\perp) \delta(p^+)),$$

$$\{b_s(p), b_{s'}^\dagger(p')\} = \{d_s(p), d_{s'}^\dagger(p')\}$$

$$= 16\pi^3 p^+ \delta^3(p - p') \delta_{ss'},$$

$$\{B_s(p), B_{s'}^\dagger(p')\} = \{D_s(p), D_{s'}^\dagger(p')\}$$

$$= 16\pi^3 p^+ \delta^3(p - p') \delta_{ss'},$$

$$\langle p_1 s_1 | p_2 s_2 \rangle = 16\pi^3 p_1^+ \delta^3(p_1 - p_2) \delta_{s_1 s_2},$$

$$|p_1 s_1\rangle = b_{s_1}^\dagger(p_1) |0\rangle, \text{ etc.}$$

APPENDIX B: BLOCH TRANSFORMATION

In this appendix we discuss a derivation of our effective Hamiltonian via a Bloch transformation [4]. We use the Bloch transformation to separate the low- and high-energy scales of the problem and derive an effective Hamiltonian acting in the low-energy space alone with an identical low-energy spectrum to the bare Hamiltonian. In this appendix, we closely follow Sec. IV of Ref. [7], where a discussion, including the original references, and derivation of a general effective Bloch Hamiltonian can be found.

We start with a bare time-independent Schrödinger equation

$$H_\Lambda |\Psi_\Lambda\rangle = E |\Psi_\Lambda\rangle. \quad (\text{B1})$$

Then projection operators onto the low- and high-energy spaces P_L and P_H , respectively, are defined,

$$P_L = \theta\left(\frac{\lambda^2 + \mathcal{P}^{\perp 2}}{\mathcal{P}^+} - h\right), \quad (\text{B2})$$

$$P_H = \theta\left(\frac{\Lambda^2 + \mathcal{P}^{\perp 2}}{\mathcal{P}^+} - h\right) \theta\left(h - \frac{\lambda^2 + \mathcal{P}^{\perp 2}}{\mathcal{P}^+}\right), \quad (\text{B3})$$

$$P_L + P_H = \theta\left(\frac{\Lambda^2 + \mathcal{P}^{\perp 2}}{\mathcal{P}^+} - h\right), \quad (\text{B4})$$

where $\theta(x)$ is a step function. Then an effective Hamiltonian acting in the low-energy space alone with an equivalent low-energy spectrum to H_Λ is sought. Λ and λ are the bare and effective cutoffs respectively with $\lambda < \Lambda$.⁶ $\mathcal{P} = (\mathcal{P}^+, \mathcal{P}^\perp)$ is the total momentum of the hydrogen state. h is the free Hamiltonian of the hydrogen system of Eq. (8).

Proceeding, a new operator \mathcal{R} is defined that connects the P_L and P_H spaces:

$$P_H |\Psi_\Lambda\rangle = \mathcal{R} P_L |\Psi_\Lambda\rangle. \quad (\text{B5})$$

More explicitly ($\sum_n |n\rangle \langle n| = 1$)

$$\mathcal{R} = \sum_{n,m} \langle n | \Psi_\Lambda \rangle \langle \Psi_\Lambda | m \rangle \frac{P_H |n\rangle \langle m| P_L}{\langle \Psi_\Lambda | P_L | \Psi_\Lambda \rangle}, \quad (\text{B6})$$

which shows that $\mathcal{R} P_H |\Psi_\Lambda\rangle = 0$ and $\mathcal{R}^\dagger P_L |\Psi_\Lambda\rangle = 0$, etc. For the construction of \mathcal{R} , see Eq. (4.4) in Ref. [7].

This leads to the following time-independent Schrödinger equation for the effective Hamiltonian:

$$H_\lambda |\Phi_\lambda\rangle = E |\Phi_\lambda\rangle. \quad (\text{B7})$$

E is the same eigenvalue as in Eq. (B1). The state $|\Phi_\lambda\rangle$ is a projection onto the low-energy space with the same norm as $|\Psi_\Lambda\rangle$ in Eq. (B1):

$$|\Phi_\lambda\rangle = \sqrt{1 + \mathcal{R}^\dagger \mathcal{R}} P_L |\Psi_\Lambda\rangle; \quad (\text{B8})$$

H_λ is a Hermitian effective Hamiltonian given by

⁶The shorthands $(\lambda^2 + \mathcal{P}^{\perp 2})/\mathcal{P}^+ \rightarrow \lambda$ and $(\Lambda^2 + \mathcal{P}^{\perp 2})/\mathcal{P}^+ \rightarrow \Lambda$ are often used when it does not lead to confusion.

$$H_\lambda = \frac{1}{\sqrt{1+\mathcal{R}^\dagger\mathcal{R}}}(P_L+\mathcal{R}^\dagger)H_\Lambda(P_L+\mathcal{R})\frac{1}{\sqrt{1+\mathcal{R}^\dagger\mathcal{R}}}. \quad (\text{B9})$$

Note that H_λ acts in the low-energy space alone. To summarize, H_λ of Eq. (B9) is guaranteed to have the same low-energy spectrum as the bare Hamiltonian H_Λ ; also, after diagonalizing H_λ , the bare state $|\Psi_\Lambda\rangle$ of Eq. (B1), if desired, is obtained through Eqs. (B8) and (B5).⁷

Defining $H_\Lambda = h + v_\Lambda$, where h is the free field theoretic Hamiltonian and v_Λ are the bare interactions,⁸ to third order in v_Λ , the effective Hamiltonian is given by

$$\begin{aligned} \langle a|H_\lambda|b\rangle &= \langle a|h+v_\Lambda|b\rangle + \frac{1}{2}\sum_i \left(\frac{\langle a|v_\Lambda|i\rangle\langle i|v_\Lambda|b\rangle}{\Delta_{ai}} \right. \\ &\quad \left. + \frac{\langle a|v_\Lambda|i\rangle\langle i|v_\Lambda|b\rangle}{\Delta_{bi}} \right) \\ &\quad + \frac{1}{2}\sum_{i,j} \left(\frac{\langle a|v_\Lambda|i\rangle\langle i|v_\Lambda|j\rangle\langle j|v_\Lambda|b\rangle}{\Delta_{ai}\Delta_{aj}} \right. \\ &\quad \left. + \frac{\langle a|v_\Lambda|i\rangle\langle i|v_\Lambda|j\rangle\langle j|v_\Lambda|b\rangle}{\Delta_{bi}\Delta_{bj}} \right) \\ &\quad - \frac{1}{2}\sum_{c,i} \left(\frac{\langle a|v_\Lambda|i\rangle\langle i|v_\Lambda|c\rangle\langle c|v_\Lambda|b\rangle}{\Delta_{bi}\Delta_{ci}} \right. \\ &\quad \left. + \frac{\langle a|v_\Lambda|c\rangle\langle c|v_\Lambda|i\rangle\langle i|v_\Lambda|b\rangle}{\Delta_{ai}\Delta_{ci}} \right) \\ &\quad + \mathcal{O}\left(\sum \langle v_\Lambda\rangle^4/(\varepsilon_{\text{high}}-\varepsilon_{\text{low}})^3\right). \quad (\text{B10}) \end{aligned}$$

$\Delta_{ia} = \varepsilon_i - \varepsilon_a$, with $h|i\rangle = \varepsilon_i|i\rangle$. We are using $|a\rangle, |b\rangle, \dots$, to denote low-energy states (states in P_L) and $|i\rangle, |j\rangle, \dots$, to denote high-energy states (states in P_H). See the already mentioned Ref. [7] for a description of an arbitrary order (in perturbation theory) effective Hamiltonian and also for a convenient diagrammatic representation of the same.

APPENDIX C: AVERAGING OVER DIRECTIONS

In this appendix we calculate the following Coulomb matrix element:

$$I_\perp = \int d^3p \int d^3p' \phi_N^*(\mathbf{p}') \frac{(\mathbf{p}^\perp - \mathbf{p}'^\perp)^2}{(\mathbf{p} - \mathbf{p}')^2} \phi_N(\mathbf{p}), \quad (\text{C1})$$

⁷This state $|\Psi_\Lambda\rangle$, will span the whole space, but will correspond to the respective low-energy eigenvalue. The bare states that correspond to the respective high-energy eigenvalues cannot be obtained from the effective Hamiltonian H_λ ; we must of course use the bare Hamiltonian H_Λ to accomplish this task.

⁸ h is written in terms of renormalized parameters, and it is convenient to define $v_\Lambda = v + \delta v_\Lambda$, where v is the canonical field theoretic interactions written in terms of renormalized parameters and δv_Λ are the counterterms that must be determined through the process of renormalization. See Eqs. (6) and (7) for the canonical Hamiltonian of the hydrogen system.

to verify the step taken from Eqs. (108) and (109) in the paper. It is useful to define another integral:

$$I_z = \int d^3p \int d^3p' \phi_N^*(\mathbf{p}') \frac{(\mathbf{p}_z - \mathbf{p}'_z)^2}{(\mathbf{p} - \mathbf{p}')^2} \phi_N(\mathbf{p}). \quad (\text{C2})$$

Now note that

$$\begin{aligned} I &= I_\perp + I_z = \int d^3p \int d^3p' \phi_N^*(\mathbf{p}') \phi_N(\mathbf{p}) \\ &= \frac{(2\pi)^3}{\pi} \left(\frac{m\alpha}{n} \right)^3 \delta_{l,0}, \quad (\text{C3}) \end{aligned}$$

where in this last step we recalled Eq. (111) and the fact that the wave function at the origin is real.

For $l=0$, the wave function satisfies

$$\phi_{n,0,0}(\mathbf{p}) = \phi_{n,0,0}(|\mathbf{p}|). \quad (\text{C4})$$

Thus, by symmetry, for $l=0$,

$$I_z = \frac{1}{3}I = \frac{(2\pi)^3}{3\pi} \left(\frac{m\alpha}{n} \right)^3, \quad (\text{C5})$$

which from Eq. (C3), for $l=0$, gives

$$I_\perp = \frac{2}{3}I = \frac{2(2\pi)^3}{3\pi} \left(\frac{m\alpha}{n} \right)^3. \quad (\text{C6})$$

For $l \neq 0$, first note that $I=0$. Thus, for $l \neq 0$,

$$I_\perp = -I_z; \quad (\text{C7})$$

we will calculate I_z below which then implies I_\perp . Next note that in position space

$$I = -2\pi^2 \int d^3x \phi_N^*(\mathbf{x}) \left(\vec{\nabla}_z^2 \frac{1}{|\mathbf{x}|} \right) \phi_N(\mathbf{x}), \quad (\text{C8})$$

using $\vec{\nabla}^2(1/|\mathbf{x}|) = -4\pi\delta^3(\mathbf{x})$. Thus, for $l \neq 0$, in position space

$$I_z = -2\pi^2 \int d^3x \phi_N^*(\mathbf{x}) \left(\vec{\nabla}_z^2 \frac{1}{|\mathbf{x}|} \right) \phi_N(\mathbf{x}). \quad (\text{C9})$$

Note that there is no $|\mathbf{x}| \rightarrow 0$ ambiguity in this previous equation because for $l \neq 0$, the wave function vanishes at the origin. Carrying out the derivative gives

$$I_z = -2\pi^2 \int d^3x \phi_N^*(\mathbf{x}) \left(\frac{-1 + 3z^2/|\mathbf{x}|^2}{|\mathbf{x}|^3} \right) \phi_N(\mathbf{x}). \quad (\text{C10})$$

This matrix element was performed in the first appendix of Bethe and Salpeter's textbook [10]. We use two of their formulas, (3.26) and (A29).⁹ Equation (C10) integrated gives

⁹Warning to the reader: In this text, they use atomic units $\hbar = c = m = \alpha = 1$, so m and α have to be placed back into the formulas.

$$I_z = -2\pi^2 \overline{r^{-3}} c(l, m_l), \quad (\text{C11})$$

with

$$\overline{r^{-3}} = \frac{1}{l(l+1)(l+1/2)} \left(\frac{m\alpha}{n} \right)^3, \quad (\text{C12})$$

$$c(l, m_l) = -1 + 3 \left(\frac{2l^2 + 2l - 1 - 2m_l^2}{(2l+3)(2l-1)} \right). \quad (\text{C13})$$

Thus, recalling Eq. (C7), our result for $l \neq 0$ is

$$I_\perp = 2\pi^2 \overline{r^{-3}} c(l, m_l). \quad (\text{C14})$$

For $l=1$, I_\perp is not 0, so what is going on? The answer lies in the fact that we really want to take matrix elements in the $|j, m_j\rangle$ basis not the $|m_l, m_s\rangle$ basis, and based on rotational invariance, our results should be independent of m_j . To proceed, note that the interactions we considered in this paper conserved m_s and our matrix elements were independent of m_s . Next, note that the result, Eq. (C14), is even under $m_l \rightarrow -m_l$. Given this, the Clebsch-Gordan coefficients for the $2P_{1/2}$ states imply

$$\langle j=1/2, m_j | V | j=1/2, m_j \rangle = \frac{1}{2l+1} \sum_{m_l=-l}^l \langle m_l | V | m_l \rangle, \quad (\text{C15})$$

where $l=1$. Now note that I_\perp given by Eq. (C14) averaged over m_l vanishes:

$$\frac{1}{2l+1} \sum_{m_l=-l}^l I_\perp = 0, \quad (\text{C16})$$

where we used

$$\frac{1}{2l+1} \sum_{m_l=-l}^l m_l^2 = \frac{1}{3} l(l+1), \quad (\text{C17})$$

an obvious result after the answer is known. This result [Eq. (C16)] was used in the step that led from Eq. (108) to Eq. (109) in the paper, and this appendix is now complete.

- [1] H. A. Bethe, Phys. Rev. **72**, 339 (1947).
 [2] B. D. Jones, R. J. Perry, and S. D. Glazek, Phys. Rev. D **55**, 6561 (1997).
 [3] K. G. Wilson, T. S. Walhout, A. Harindranath, W. M. Zhang, R. J. Perry, and S. D. Glazek, Phys. Rev. D **49**, 6720 (1994).
 [4] C. Bloch, Nucl. Phys. **6**, 329 (1958).
 [5] R. J. Perry, in *Hadrons 94*, Proceedings of Workshop, Gramado, Brazil, edited by V. Herscovitz and C. Vasconcellos (World Scientific, Singapore, 1995), hep-th/9407056; M. M. Brisudová and R. J. Perry, Phys. Rev. D **54**, 1831 (1996); M. M. Brisudová, Report No. hep-ph/9604386, 1996 (unpublished); M. M. Brisudová, R. J. Perry, and K. G. Wilson, Phys. Rev. Lett. **78**, 1227 (1997).
 [6] R. J. Perry and K. G. Wilson, Nucl. Phys. **B403**, 587 (1993); R. J. Perry, Ann. Phys. (N.Y.) **232**, 116 (1994), p. 123 (for further comments on coupling coherence, see the paragraph containing Eq. (39) of Ref. [2]).
 [7] R. J. Perry, Ann. Phys. (N.Y.) **232**, 116 (1994), Sec. IV.
 [8] R. W. Huff, Phys. Rev. **186**, 1367 (1969), Table II, p. 1372 (note the typo: $2Y \rightarrow 2S$).
 [9] Particle Data Group, R. M. Barnett *et al.*, Phys. Rev. D **54**, 1 (1996).
 [10] H. A. Bethe and E. E. Salpeter, *Quantum Mechanics of One- and Two-Electron Atoms* (Plenum, New York, 1977), pp. 17 and 348.